

Critical Anisotropies of a Geometrically-Frustrated Triangular-Lattice Antiferromagnet

M. Swanson^{1,2}, J.T. Haraldsen¹, and R.S. Fishman¹

¹Materials Science and Technology Division, Oak Ridge National Laboratory, Oak Ridge, Tennessee 37831, USA

²North Dakota State University, Fargo, North Dakota 58105, USA

(Dated: February 21, 2024)

This work examines the critical anisotropy required for the local stability of the collinear ground states of a geometrically-frustrated triangular-lattice antiferromagnet (TLA). Using a Holstein-Primakoff expansion, we calculate the spin-wave frequencies for the 1, 2, 3, 4, and 8-sublattice (SL) ground states of a TLA with up to third neighbor interactions. Local stability requires that all spin-wave frequencies are real and positive. The 2, 4, and 8-SL phases break up into several regions where the critical anisotropy is a different function of the exchange parameters. We find that the critical anisotropy is a continuous function everywhere except across the 2-SL/3-SL and 3-SL/4-SL phase boundaries, where the 3-SL phase has the higher critical anisotropy.

Introduction. Geometrically-frustrated systems exhibit many novel characteristics including non-collinear ground states and multiferroic properties¹. One of the best realizations of a geometrically-frustrated triangular-lattice antiferromagnet (TLA) is CuFeO_2 , which contains stacked hexagonal planes of spin-5/2 Fe^{3+} ions. Accompanied by a phase transition from a collinear 4-sublattice (SL) ground state to a non-collinear phase^{2,3,4,5}, CuFeO_2 exhibits multiferroic properties above a critical magnetic field or above a critical concentration of non-magnetic Al^{3+} impurities, which substitute for the Fe^{3+} ions^{6,7}. Inelastic neutron-scattering experiments^{8,9,10} on CuFeO_2

have reported a spin-wave (SW) gap of about 0.9 meV, which decreases with Al doping and may vanish¹¹ upon the appearance of multiferroic behavior. Similar behavior is produced in a model TLA as the anisotropy is reduced¹² and spin fluctuations about the 4-SL collinear phase become stronger. In this paper, we evaluate the critical anisotropies required for the local stability of the collinear magnetic phases in a model TLA with up to third nearest neighbors. As shown elsewhere¹³, the wave-vector of the dominant SW instabilities of a collinear phase coincide with the dominant wave-vector of the non-collinear phase that appears with decreasing anisotropy. Therefore, an analysis of the critical anisotropies and wave-vectors of a frustrated TLA can provide useful information about the non-collinear phases that appear at small anisotropy.

The collinear ground states of a TLA with strong anisotropy were first obtained by Takagi and Makata¹⁴, who examined an Ising model with interactions up to third nearest neighbors. The ground-state phase diagram consists of the five phases sketched in Fig. 1, where the energies of these five states are given in Table I. Using a Holstein-Primakoff (HP) expansion, we have calculated the SW frequencies and critical anisotropies for each of these phases.

The Hamiltonian for a TLA is given by

$$H = \frac{1}{2} \sum_{i \neq j} J_{ij} S_i \cdot S_j + D \sum_i S_{iz}^2; \quad (1)$$

where S_i is the local moment on site i , J_{ij} is the interaction between sites i and j , and D is the single-ion anisotropy. Employing a HP transformation, the spin operators are given by $S_{iz} = S - a_i^\dagger a_i$, $S_{i+} = \sqrt{2S} a_i$, and $S_{i-} = \sqrt{2S} a_i^\dagger$. Expanded about the classical limit in powers of $1/S$, the Hamiltonian can be written as $H = E + H_1 + H_2 + \dots$. The first-order term H_1 vanishes when the spin configuration minimizes the energy E . The second-order term H_2 provides the dynamics of non-interacting SWs. Higher-order terms $H_{n>2}$ reflect the interactions between SWs. They are unimportant

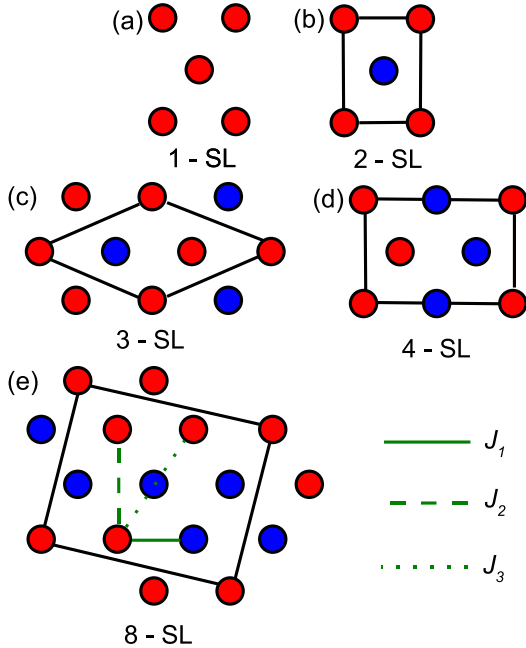


FIG. 1: (Color online) The 1, 2, 3, 4, and 8-SL phases for the ground states of the geometrically-frustrated TLA. The solid black lines denote the magnetic unit cell of each phase. Up and down spins are designated by red and blue circles, respectively.

at low temperature and for large $l=S$. Similar to Takagi and Makata, we consider nearest neighbor J_1 , next-nearest neighbor J_2 , and next-next-nearest-neighbor J_3 exchange interactions, as sketched in Fig. 1.

To determine the SW frequencies ω_k , we solve the equation-of-motion for the vectors $v_k = [a_k^{(1)}; a_k^{(1)y}; a_k^{(2)}; a_k^{(2)y}; \dots]$, which may be written in terms of the $2N \times 2N$ matrix $\underline{M}(k)$ as $i\partial_t v_k = \underline{M}(k)v_k$, where N is the number of spin sites in the unit cell. The SW frequencies are then determined from the condition $\det \underline{M}(k) = 0$.

Two conditions are required for the local stability of any magnetic phase: all SW frequencies must be real and positive and all SW weights must be positive. The SW weights $W_k^{(s)}$ are coefficients of the spin-spin correlation function:

$$S(k; \omega) = \frac{1}{N} \int dt e^{i\omega t} \sum_{ij} e^{ik \cdot d_{ij}} S_i^+ S_j(t) + S_i S_j^+(t) = \sum_s W_k^{(s)}(\omega) S_i^{(s)} S_j^{(s)}; \quad (2)$$

where s denotes a branch of the SW spectrum and d_{ij} is defined as the vector pointing from site i to site j . The weights $W_k^{(s)}$ were evaluated within the HP formalism by solving the equations-of-motion for coupled spin Green's functions^{15,16}. In zero field, the condition that the SW weights are positive for all k is equivalent to the condition that all SW frequencies are positive.

We obtained analytic expressions for the SW frequencies for all phases shown in Fig. 1 with the exception of the 8-SL phase, which was solved numerically. A analysis of the SW frequencies yields the critical anisotropy D_c and the critical wave-vectors k where the SW frequencies vanish. To simplify the following discussion, the SW and anisotropy coefficients are provided in the appendix.

1-Sublattice. The 1-SL phase (Fig. 1(a)) is a ferromagnet with SW frequencies

$$\omega_k^{(1)} = 2S(D + A_{1k}) \quad (3)$$

Since the 1-SL phase is locally stable for any positive value of the anisotropy, $D_c = 0$. The SW intensity $W_k^{(1)}$ is constant throughout k for all interactions.

2-Sublattice. For the 2-SL phase (shown in Fig. 1(b)), the SW frequencies are given by

$$\omega_k^{(2)} = 2S \sqrt{A_{2k}^2 + A_{3k}^2} \quad (4)$$

The SW weights for the 2-SL phase are

$$W_k^{(2)} = \frac{r}{A_{2k} + A_{3k}} \quad (5)$$

From Eq. (4), the condition for the local stability of a 2-SL phase is $A_{2k}^2 + A_{3k}^2 > 0$. At D_c , $A_{2k}^2 = A_{3k}^2$.

TABLE I: Classical Energies and Critical Anisotropies for TLA Sublattices

SL	Energy	D_c
1-SL	$\frac{E^{(1)}}{N S^2} = J_1 + J_2 + J_3 + D$	$D_c^{(1)} = 0$
2-SL	$\frac{E^{(2)}}{N S^2} = J_1 + J_2 + J_3 + D$	$D_c^{(2I)} \text{ (Eq. (6))}$ $D_c^{(2II)} \text{ (Eq. (8))}$ $D_c^{(2III)} \text{ (Eq. (9))}$ $D_c^{(2IV)} = 0$
3-SL	$\frac{E^{(3)}}{N S^2} = J_1 + J_2 + J_3 + D$	$D_c^{(3)} \text{ (Eq. (15))}$
4-SL	$\frac{E^{(4)}}{N S^2} = J_1 + J_2 + J_3 + D$	$D_c^{(4I)} \text{ (Eq. (18))}$ $D_c^{(4II)} \text{ (Eq. (19))}$
8-SL	$\frac{E^{(8)}}{N S^2} = J_2 + J_3 + D$	$D_c^{(8I)} \text{ (Eq. (20))}$ $D_c^{(8II)} \text{ (Eq. (21))}$

This condition is satisfied when $D_c = 0$ in most of the 2-SL phase. But approaching the 3, 4, and 8-SL phase boundaries, nonzero anisotropy is required for local stability. As shown in Fig. 3(a), the critical anisotropy is continuous across the 4-SL and 8-SL boundaries, but is discontinuous across the 3-SL boundary.

Upon closer examination (Fig. 3(c)), we find that D_c depends differently on the exchange parameters in the three regions designated by Roman numerals. In region 2I (bounded by $J_3 = J_2=2$, $J_3 = (9J_2 - J_1)=12$, and $J_3 = J_2^2=(J_1 - 2J_2)$),

$$D_c^{(2I)} = \frac{1}{(4J_3)^3} \left(272J_3^4 + 64J_3^3J_2 + 48J_3^3J_1 + 72J_3^2J_2^2 + 48J_3^2J_2J_1 + 8J_3^2J_1^2 + 36J_3J_2^2J_1 + 27J_2^4 + (2J_3 - J_2)C^3 \right); \quad (6)$$

where

$$C = \frac{P}{(2J_3 + 3J_2)^2 - 8J_3J_1} \quad (7)$$

In region 2II (bounded by $J_3 = J_2=2$, $J_3 = J_2$, $J_3 = (8J_2 - J_1)=9$, and $J_3 = J_2^2=(J_1 - 2J_2)$),

$$D_c^{(2II)} = 4J_2 - \frac{9}{2}J_3 - \frac{1}{2}J_1; \quad (8)$$

Finally, in region 2III (bounded by $J_3 = J_2=2$, $J_3 = J_1=4$,

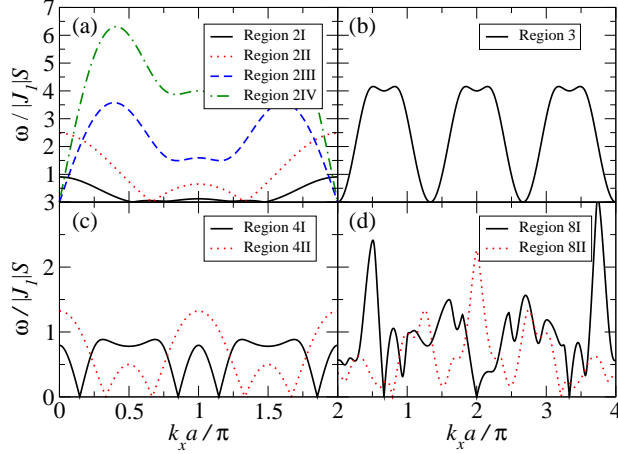


FIG. 2: (Color online) SW frequencies at the critical anisotropy for 2 (a), 3 (b), 4 (c), and 8-SL (d) phases (interaction parameters given in the text). All SW instabilities occur for $k_y a = 0$ except in regions 2III and 8I, where they occur for $k_y a = 0.186$ and 0.382 , respectively.

and $J_3 = (J_1 - J_2) = 4$,

$$D_c^{(2III)} = \frac{(4J_3 + J_2 - J_1)^2}{2(J_2 + 2J_3)}; \quad (9)$$

The region with no critical anisotropy $D_c^{(2IV)}$ is bounded by $J_2 = 0$, $J_3 = (8J_2 - J_1) = 9$, and $J_3 = (J_1 - J_2) = 4$ as shown in Figs. 3(b) and (c).

The critical wave-vectors, k for the SW instabilities in region 2I are:

$$k_x^{(2I;a)} a = 2 \arccos \frac{3J_2 - 2J_3 - C}{8J_3}; \quad (10)$$

$$k_y^{(2I;a)} a = 0;$$

Two other instabilities $k^{(2I;b)}$ and $k^{(2I;c)}$ are related to $k^{(2I;a)}$ by $\pi/3$ rotations and can be considered "twins" of the $k^{(2I;a)}$ instabilities. All three instabilities occur at the same critical anisotropy $D_c^{(2I)}$. For regions 2II and III, the SW instabilities occur at

$$k_x^{(2II)} a = \pi/3; \quad (11)$$

$$k_y^{(2II)} a = 0;$$

and

$$k_x^{(2III)} a = 0; \quad (12)$$

$$k_y^{(2III)} a = \frac{2}{\pi} \arccos \frac{J_2 + J_1}{2(J_2 + 2J_3)};$$

along the k_x and k_y axis, respectively.

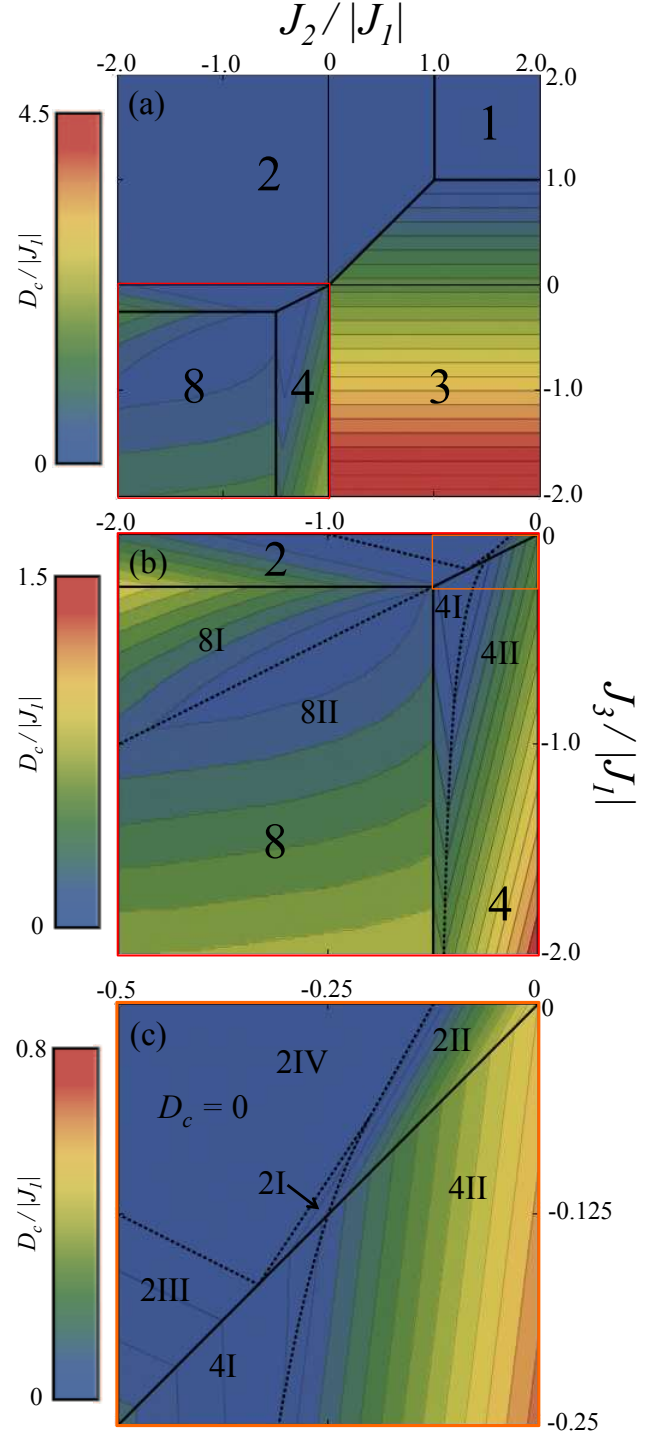


FIG. 3: (Color online) Critical anisotropies for the TLA ground states. The spacing between contours is 0.2 (a), 0.1 (b), and 0.05 (c). Numbers designate the stable phase and Roman numerals designate regions where the behavior of the critical anisotropy is distinct. Solid lines denote boundaries between phases and dashed lines denote boundaries between regions. D_c is continuous across each phase boundary except for the 2-SL/3-SL and the 3-SL/4-SL phase boundaries; in both cases, D_c is higher for the 3-SL phase.

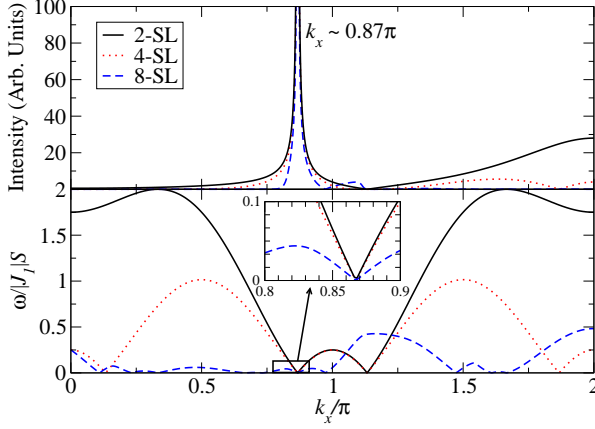


FIG. 4: (Color online) SW frequencies and SF intensities for the 2, 4, and 8-SL phases at the critical anisotropy with $J_2 = J_1 J = 0.5$, $J_3 = J_1 J = 0.25$, and $D = J_1 J = 0.125$.

Figure 2(a) shows three representative SWs for all 2-SL regions. The interaction parameters for region 2I are $J_2 = J_1 J = 0.25$, $J_3 = J_1 J = 0.12$, and $D_c = J_1 J = 0.04$. For region 2II, $J_2 = J_1 J = 0.10$, $J_3 = J_1 J = 0.05$, and $D_c = J_1 J = 0.325$. For region 2III, $J_2 = J_1 J = 0.75$, $J_3 = J_1 J = 0.125$, and $D_c = J_1 J = 0.031$. Finally, for region IV, the interaction parameters are $J_2 = J_1 J = 1.0$, $J_3 = J_1 J = 0.125$, and $D_c = J_1 J = 0.0$. Regions I, II and IV were evaluated with $k_y a = 0$, while region III was evaluated at $k_y a = 0.186$ as explained above.

In Figs. 3(b) and (c), we examine the critical anisotropy of the 2-SL along the $J_3 = J_1 J = 0$ axis. The critical anisotropy vanishes for $1 < J_2 = J_1 J < 1.8$ but is nonzero outside this region. Therefore, non-collinear phases should appear for $J_2 = J_1 J < 1$ and $J_2 = J_1 J > 1.8$ when $D < D_c$. This agrees with Jolicoeur et al.¹⁷, who studied a TLA with nearest and next-nearest neighbor exchange interactions and $D = 0$. They obtain a Neel state up to $J_2 = J_1 J = 1.8$ and an incommensurate spiral for $J_2 = J_1 J < 1$. Similar results have been obtained on square lattices^{18,19}.

3-Sublattice. For the 3-SL phase (shown in Fig. 1(c)), the SW frequencies are

$$\omega_k^{(3)} = 6S \frac{P}{R_{1k}} \cos(\pi/3 + 2m\pi/3) + R_{2k} = 3; \quad (13)$$

where m is an integer (0,1,2) distinguishing the three separate SW dispersion relations and

$$P = \arccos \left(\frac{2R_{2k}^3 - 9R_{2k}R_{3k} + 27R_{4k}}{1458R_{1k}^{3/2}} \right); \quad (14)$$

The critical anisotropy of the 3-SL phase is independent of J_2 and given by

$$D_c^{(3)} = \frac{3}{2} (J_1 + J_3); \quad (15)$$

Notice and that $D_c^{(3)} = 0$ along the 3-SL/1-SL boundary. Again, D_c is discontinuous along the 2-SL/3-SL and 3-SL/4-SL boundaries: the anisotropy required for the local stability of the 3-SL phase is three times the critical anisotropy of the 2 or 4-SL phases. As discussed further below, the discontinuities at the 2-SL/3-SL and 3-SL/4-SL phase boundaries are related to the distinction between the conditions for global and local stability.

In Fig. 2(b), we plot a SW dispersion in the 3-SL phase with interaction parameters $J_2 = J_1 J = 0.5$, $J_3 = J_1 J = 0.5$, and $D_c = J_1 J = 2.25$. Since the 3-SL phase has a net moment, the SW frequencies are quadratic functions of k near the instability wave-vectors.

4-Sublattice. The SW frequencies for the 4-SL phase (shown in Fig. 1(d)) were evaluated in Ref. [12] and are given by

$$\omega_k^{(4)} = 2S \frac{h}{A_{6k}^2 A_{7k}^2 F_{2k}^2 F_{2k}^2} + 4 \frac{A_{6k} F_{2k} A_{7k} F_{2k}}{J_{1=2}^2 J_{1=2}^2}; \quad (16)$$

The SW weights of the 4-SL phase are

$$W_k^{(4)} = R_{5k} \frac{h}{(A_{7k} A_{6k}) + (F_{2k} + F_{2k})(A_{6k} A_{7k})^2} + (F_{2k} F_{2k})^2 (F_{2k} + F_{2k} A_{6k} A_{7k}) \frac{i}{R_{5k} \frac{p}{A_{6k}^2 A_{7k}^2 R_{5k}} i_1}; \quad (17)$$

As for the 2-SL phase, the critical anisotropy D_c for the 4-SL phase depends differently on the interaction parameters in two regions, again denoted by Roman numerals I and II (Fig. 3(b)). In region 4I (bounded by $J_3 = J_2 = 2$, $J_2 = J_1 = 2$, and $J_3 = J_2^2 = (J_1 - 2J_2)$),

$$D_c^{(4I)} = \frac{1}{(4J_3)^3} \left(16J_3^4 - 64J_3^3 J_2 + 48J_3^3 J_1 + 72J_2^2 J_3^2 - 8J_3^2 J_1^2 - 48J_3^2 J_2 J_1 + 36J_3 J_2^2 J_1 - 27J_2^4 + (2J_3 - J_2)C^3 \right); \quad (18)$$

and in region 4II (bounded by $J_3 = J_2 = 2$, $J_2 = 0$, and $J_3 = J_2^2 = (J_1 - 2J_2)$),

$$D_c^{(4II)} = 2J_2 - \frac{1}{2}J_3 - \frac{1}{2}J_1; \quad (19)$$

The critical wave-vectors for the 4-SL phase are the same as those in the respective region of the 2-SL phase, including the multiple instabilities in region 2I: $k^{(4Ia)} = k^{(2Ia)}$, $k^{(4Ib)} = k^{(2Ib)}$, and $k^{(4II)} = k^{(2II)}$. Figure 2(c) shows two representative SWs for regions 4I and 4II with $k_y a = 0$. The interaction parameters for region 4I are $J_2 = J_1 J = 0.439$, $J_3 = J_1 J = 0.570$, and $D_c = J_1 J = 0.105$. For region 4II, they are $J_2 = J_1 J = 0.25$, $J_3 = J_1 J = 0.5$, and $D_c = J_1 J = 0.25$.

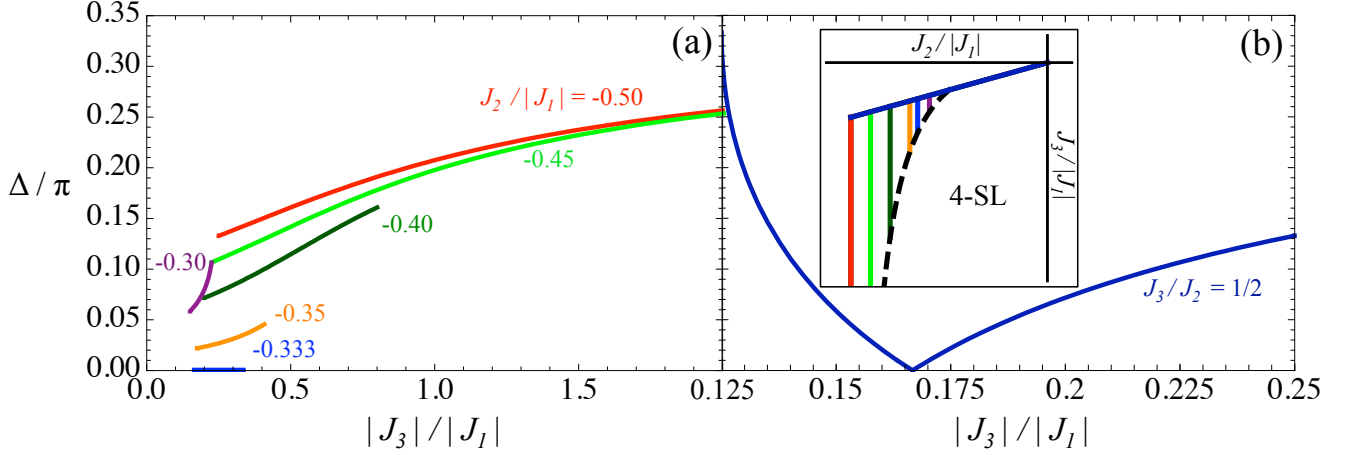


FIG. 5: (Color online) (a) Location of SW instability $\Delta = \mathbf{a} \cdot \mathbf{k}_x - \mathbf{j}$ along $k_y a = 0$ in region 4I for fixed values of $J_2 = \mathbf{j}J_1 \mathbf{j}$. As $\mathbf{j}J_3 = \mathbf{j}J_1 \mathbf{j}$ increases along $J_2 = \mathbf{j}J_1 \mathbf{j} = 0.5$, asymptotically approaches $\Delta = 3$. (b) Plot of Δ in region 4I along the 2-SL/4-SL boundary $J_3 = J_2 = 1/2$. The cusp in Δ occurs at $J_2 = \mathbf{j}J_1 \mathbf{j} = 1/3$ where the SW instability occurs at $\Delta = 3$.

Figure 4 shows the SW frequencies and SF intensities for the 2, 4, and 8-SL phases at the triple point of the phase diagram. The intensities for the 8-SL phase were determined numerically. As shown in Fig. 4, each phase becomes unstable at $D = \mathbf{j}J_1 \mathbf{j} = 0.125$, where the SW intensity for each phase peaks at the same wave-vector. This wave-vector corresponds to the ordering wave-vector of the non-collinear phase¹³ that appears at small anisotropy. Because the 2, 4, and 8-SL phases all have zero net moment, their SW frequencies are linear functions of k around the wave-vectors of the instabilities.

The 4-SL phase is of particular interest since it is the known ground state² of CuFeO_2 . Fits of the experimental SW frequencies^{8,15} of CuFeO_2 have determined the ratios of exchange parameters $J_2 = \mathbf{j}J_1 \mathbf{j} = 0.44$ and $J_3 = \mathbf{j}J_1 \mathbf{j} = 0.57$, which lies within region 4I. Consequently, we have studied the SW frequencies of the 4-SL phase more closely. Figure 5 shows the behavior of $k_x^{(4I,a)}$ along various cuts through region 4I of phase space. Since the SW frequencies are symmetric about the midpoint of the Brillouin zone \mathbf{a} , we consider the quantity $\Delta = \mathbf{a} \cdot \mathbf{k}_x - \mathbf{j}$. As $J_3 = \mathbf{j}J_1 \mathbf{j}$ increases in region 4I, asymptotically approaches $\Delta = 3$, which is the constant value of Δ in region 4II. For small values of $J_3 = \mathbf{j}J_1 \mathbf{j}$ the wave-vector instabilities approach $\Delta = 3$ as $J_2 = \mathbf{j}J_1 \mathbf{j}$ increases, equal for $J_2 = \mathbf{j}J_1 \mathbf{j} = 1/3$, and then move away from $\Delta = 3$ as $J_2 = \mathbf{j}J_1 \mathbf{j}$ approaches zero; this behavior is shown along the 2-SL/4-SL boundary in Fig. 5(b).

8-Sublattice. For the 8-SL phase (shown in Fig. 1(e)), we have determined SW dispersion relations numerically. The critical anisotropy values for this phase are shown in Fig. 3(a). Notice that D_c has a cusp dividing the phase into regions 8I and 8II (Fig. 3(b)), separated by $J_3 = J_2 = 2$. Looking more closely at the numerical results, the critical anisotropies in the 8-SL regions are closely related

to those of their respective neighbors and are given by

$$D_c^{(8I)} = D_c^{(2III)} + 4J_3 - J_1; \quad (20)$$

$$D_c^{(8II)} = D_c^{(4I)} + 2J_2 - J_1; \quad (21)$$

which clearly show that the critical anisotropies are continuous across the phase boundaries. In region 8II, the wave-vector instabilities occur for $k_y = 0$ (as in region 4I); in region 8I, the wave-vector instabilities occur for non-zero k_y (as in region 2III). Figure 2(d) shows two representative SWs for regions 8I and 8II. The interaction parameters for region 8I are $J_2 = \mathbf{j}J_1 \mathbf{j} = 1.5$, $J_3 = \mathbf{j}J_1 \mathbf{j} = 0.50$, and $D_c = \mathbf{j}J_1 \mathbf{j} = 0.25$. For region 8II, they are $J_2 = \mathbf{j}J_1 \mathbf{j} = 0.75$, $J_3 = \mathbf{j}J_1 \mathbf{j} = 0.50$, and $D_c = \mathbf{j}J_1 \mathbf{j} = 0.62$. Whereas $k_y a = 0$ for region 8II, $k_y a = 0.382$ for region 8I as explained above.

To better understand the discontinuities along the 2-SL/3-SL and 3-SL/4-SL phase boundaries, we consider the relationship between local and global stability. Our SW calculations only guarantee the local stability of each collinear phase. But even when a phase is locally stable, it can still be globally unstable to a lower-energy spin configuration. Hence, the critical anisotropy D_c for global stability must be greater than or equal to the critical anisotropy D_c for local stability. Unlike D_c , D_c^* must also be a continuous function of J_1 , J_2 , and J_3 . So when D_c is discontinuous, the phase with the lower critical anisotropy cannot be globally stable. Since the 3-SL has a higher critical anisotropy along the 2 and 4-SL boundaries, the 2-SL and 4-SL phases cannot be globally stable along those boundaries when $D_c^{(2II)} < D < D_c^{(3)}$ or $D_c^{(4II)} < D < D_c^{(3)}$. Therefore, our results for the local stability of the collinear phases also has implications for the global stability of those phases.

Conclusion. We have examined the critical anisotropy for a geometrically-frustrated TLA. Based on the Takagi-Makata phase diagram, we calculated the SW frequencies

for all wave phases. Imposing the two conditions for local stability, we obtained the critical anisotropies and wave-vector instabilities for all phases as functions of the exchange interactions. Surprisingly, these results are highly dependent on the longer-range exchange interactions and most phases break into several regions where the anisotropy has a distinct dependence on the exchange parameters. As discussed for the 2-SL and 4-SL phases, the critical anisotropies and wave-vectors for the local stability of the collinear phases provides useful information about the non-collinear phases that appear at small anisotropy. We have also shown that the discontinuity of the critical anisotropy at the 2-SL/3-SL and 3-SL/4-SL phase boundaries has implications for the global stability of the 2-SL and 4-SL phases with the smaller critical anisotropies.

We would like to acknowledge helpful conversations with Gonzalo Alvarez. This research was sponsored by the Laboratory Directed Research and Development Program of Oak Ridge National Laboratory, managed by UT-Battelle, LLC for the U.S. Department of Energy under contract No. DE-AC05-00OR22725 and by the Division of Materials Science. We would also like to acknowledge the DOE SULI program for support during this research.

APPENDIX A: SPIN-WAVE AND ANISOTROPY COEFFICIENTS

This Appendix provides the coefficients that enter the SW frequencies and weights for each phase. The coefficients for the 1-SL or ferromagnetic phase are

$$A_{1k} = 3(J_1 + J_2 + J_3)$$

$$J_1 \cos(k \cdot \mathbf{q}) + \cos(k \cdot \mathbf{q}) + \cos(k \cdot \mathbf{q})$$

$$J_2 \cos(k \cdot \mathbf{q}) + \cos(k \cdot \mathbf{q}) + \cos(k \cdot \mathbf{q})$$

$$J_3 \cos(2k \cdot \mathbf{q}) + \cos(2k \cdot \mathbf{q}) + \cos(2k \cdot \mathbf{q}); \quad (\text{A } 1)$$

where $d_1 = ax, d_2 = \frac{1}{\sqrt{3}}ax + \frac{2}{\sqrt{3}}ay, d_3 = \frac{1}{\sqrt{3}}ax + \frac{2}{\sqrt{3}}ay, d_4 = \frac{2}{\sqrt{3}}ax + \frac{1}{\sqrt{3}}ay, d_5 = \frac{2}{\sqrt{3}}ax + \frac{1}{\sqrt{3}}ay$, and $d_6 = \frac{2}{\sqrt{3}}ax + \frac{1}{\sqrt{3}}ay$.

The 2-SL phase coefficients are

$$A_{2k} = D + 3J_3$$

$$J_1 \cos(k \cdot \mathbf{q}) + 1 - J_2 \cos(k \cdot \mathbf{q}) + 1$$

$$J_3 \cos(2k \cdot \mathbf{q}) + \cos(2k \cdot \mathbf{q}) + \cos(2k \cdot \mathbf{q}); \quad (\text{A } 2)$$

$$A_{3k} = J_1 \cos(k \cdot \mathbf{q}) + \cos(k \cdot \mathbf{q}) + J_2 \cos(k \cdot \mathbf{q}) + \cos(k \cdot \mathbf{q}); \quad (\text{A } 3)$$

The 3-SL phase coefficients are

$$R_{1k} = R_{2k}^2 - 3R_{3k}; \quad (\text{A } 4)$$

$$R_{2k} = 2A_{4k} + A_{5k}; \quad (\text{A } 5)$$

$$R_{3k} = A_{4k}^2 + 2A_{4k}A_{5k} + F_{1k}^2; \quad (\text{A } 6)$$

$$R_{4k} = (A_{5k} - 2A_{4k})F_{1k}^2 - A_{4k}^2A_{5k} - F_{1k}^3 - F_{1k}^3; \quad (\text{A } 7)$$

$$A_{4k} = 2D + 2J_2(3 \cos(k \cdot \mathbf{q}) \cos(k \cdot \mathbf{q}) - \cos(k \cdot \mathbf{q}) - \cos(k \cdot \mathbf{q})); \quad (\text{A } 8)$$

$$A_{5k} = 6J_1 + 6J_3 - A_{3k}; \quad (\text{A } 9)$$

$$F_{1k} = J_1(e^{ik \cdot d_2} + e^{ik \cdot d_1} + e^{ik \cdot d_3}) + J_3(e^{2ik \cdot d_2} + e^{2ik \cdot d_1} + e^{2ik \cdot d_3}); \quad (\text{A } 10)$$

As in Ref.(12), the 4-SL phase coefficients are

$$R_{5k} = F_{2k}^4 + F_{2k}^4 - 2(F_{2k}^2 + 2A_{6k}A_{7k})F_{2k}^2 + 4(A_{6k}^2 + A_{7k}^2)F_{2k}^2 - 4A_{6k}A_{7k}F_{2k}^{1=2}; \quad (\text{A } 11)$$

$$A_{6k} = D - J_1 + J_2(1 - \cos(k \cdot \mathbf{q}) - J_3(1 + \cos(2k \cdot \mathbf{q}))); \quad (\text{A } 12)$$

$$A_{7k} = \cos(k \cdot \mathbf{q}) - J_1 + 2J_3 \cos(\frac{2}{\sqrt{3}}k \cdot \mathbf{q}); \quad (\text{A } 13)$$

$$F_{2k} = \cos(k \cdot \mathbf{q}) - J_1 e^{ik \cdot d_1} + J_2 e^{3ik \cdot d_1}; \quad (\text{A } 14)$$

-
- ¹ See, for example, *Frustrated Spin Systems* (World Scientific, New Jersey, 2004), edited by H. T. Diep.
 - ² S. M. Ito, H. Yoshizawa, N. Yaguchi, and M. Mekata, *J. Phys. Soc. Jpn.* **60**, 1885 (1991).
 - ³ M. Mekata, N. Yaguchi, T. Takagi, T. Sugino, S. M. Ito, H. Yoshizawa, N. Hosito, and T. Shinjo, *J. Phys. Soc. Jpn.* **12**, 4474 (1993).
 - ⁴ O. A. Petrenko, M. R. Lees, G. Balakrishnan, S. de Brion, and G. Chouteau, *J. Phys.: Condens. Matter* **17**, 2741 (2005).
 - ⁵ N. Terada, Y. Nanami, K. Katsumata, T. Yamamoto, U. Staub, K. Kondo, M. Hagiwara, Y. Tanaka, A. Kikkawa, H. Toyokawa, T. Fukui, R. Kanmuri, T. Ishikawa, and H. Kikuchi, *Phys. Rev. B* **74**, 180404(R) (2006).
 - ⁶ N. Terada, S. M. Ito, T. Fujii, K. Soejima, I. Doi, H. Aruga Katori, and Y. Noda, *J. Phys. Soc. Jpn.* **74**, 2604 (2005).
 - ⁷ S. Seki, Y. Yamasaki, Y. Shiomi, S. Iguchi, Y. Onose, and Y. Tokura, *Phys. Rev. B* **75**, 100403(R) (2007).
 - ⁸ F. Ye, J. A. Fernandez-Baca, R. S. Fishman, Y. Ren, H. J. Kang, Y. Qiu, and T. Kikuchi, *Phys. Rev. Lett.* **99**, 157201 (2007).
 - ⁹ N. Terada, S. M. Ito, Y. Ohara, H. Yoshizawa, and H. Takei, *J. Magn. Mater.* **272-276**, e997 (2004).
 - ¹⁰ T. Kikuchi, J. C. Lashley, and A. P. Ramirez, *Phys. Rev. B* **73**, 220401(R) (2006).
 - ¹¹ N. Terada, S. M. Ito, T. Fujii, D. Petitgrand, *J. Phys.: Condens. Matter* **19**, 145241 (2007).
 - ¹² R. S. Fishman, *J. Appl. Phys.* **103**, 07B109 (2008).
 - ¹³ J. T. Haraldsen, M. Swanson, G. Alvarez, and R. S. Fishman, *arXiv:0901.2336v1* (2009).
 - ¹⁴ T. Takagi and M. Mekata, *J. Phys. Soc. Jpn.* **64**, 4609 (1995).
 - ¹⁵ R. S. Fishman, F. Ye, J. A. Fernandez-Baca, J. T. Haraldsen, and T. Kikuchi, *Phys. Rev. B* **78**, 140407(R) (2008).
 - ¹⁶ J. T. Haraldsen and R. S. Fishman, *arXiv:0901.2332v1* (2009).
 - ¹⁷ Th. Jolicoeur, E. Dagotto, E. Dagliano, and S. Bacci, *Phys. Rev. B* **42**, 4800 (1990).
 - ¹⁸ E. Dagotto and A. Moreo, *Phys. Rev. Lett.* **63**, 2148 (1989).
 - ¹⁹ P. Chandra and B. Doucot, *Phys. Rev. B* **38**, 9335 (1988).